Proc. Natl. Acad. Sci. USA
Vol. 85, pp. 3304–3308, May 1988
Biochemistry

Structural analysis of a series of antiviral agents complexed with human rhinovirus 14

JOHN BADGER*, IWONA MINOR*, MARCIA J. KREMER*, MARCOS A. OLIVEIRA*, THOMAS J. SMITH*, JAMES P. GRIFFITH*, DIEGO M. A. GUERIN*, S. KRISHNASWAMY*, MING LUO*, MICHAEL G. ROSSMANN*, MARK A. MCKINLAY†, GUY D. DIANA†, FRANK J. DUTKO†, MARILYN FANCHER†, ROLAND R. RUECKERT‡, AND BEVERLY A. HEINZ‡

*Department of Biological Sciences, Purdue University, West Lafayette, IN 47907; †Sterling–Winthrop Research Institute, Columbia Turnpike, Rensselaer, NY 12144; and ‡Institute for Molecular Virology, University of Wisconsin, 1525 Linden Drive, Madison, WI 53706

Contributed by Michael G. Rossmann, January 11, 1988

ABSTRACT **The binding to human rhinovirus 14 of a series of eight antiviral agents that inhibit picornaviral uncoating after entry into host cells has been characterized crystallographically. All of these bind into the same hydrophobic pocket within the viral protein VP1 β-barrel structure, although the orientation and position of each compound within the pocket was found to differ. The compounds cause the protein shell to be less flexible, thereby inhibiting disassembly. Although the antiviral potency of these compounds varies by 120-fold, they all induce the same conformational changes on the virion. The interactions of these compounds with the viral capsid are consistent with their observed antiviral activities against human rhinovirus 14 drug-resistant mutants and other rhinovirus serotypes. Crystallographic studies of one of these mutants confirm the partial sequencing data and support the finding that this is a single mutation that occurs within the binding pocket.**

Picornaviruses are small RNA-containing animal viruses with molecular masses of approximately 8.5×10^6 daltons (of which about 30% is due to RNA) and with external diameters of about 300 Å. This family of viruses is responsible for diseases including the common cold, hepatitis A, poliomyelitis, and foot-and-mouth disease. Structures for the human rhinovirus (1), poliovirus (2) and Mengo virus (3) have been determined by x-ray crystallographic analysis to about 3 Å resolution. The protein capsid of these viruses is composed of 60 protomers in an icosahedrally symmetric arrangement. Each protomer is composed of three surface viral proteins (VP1, VP2, and VP3) and a smaller internal protein (VP4). The three larger proteins are folded into eight-stranded antiparallel β-barrel structures and form a pseudo $T = 3$ (T = triangulation number) surface lattice. Surrounding each of the 12 pentamer axes on the rhinovirus surface is a 25 Å deep canyon with four neutralizing immunogen sites on either rim of the canyon. The neutralizing immunogen sites are hypervariable between different rhinovirus serotypes, while the canyon floor is relatively well conserved. It has been proposed that the canyon is the site of the receptor attachment for the virus (1).

A series of structurally related antiviral compounds (Fig. 1) synthesized at the Sterling–Winthrop Research Institute and designated "WIN compounds" (4) has been found to inhibit picornaviral replication by preventing uncoating (5), as have some other structurally unrelated compounds (6, 7). We have examined the binding of some of these compounds to human rhinovirus 14 (HRV14) in an extension of the work reported by Smith *et al.* (8). All of these compounds bind into a hydrophobic pocket beneath the canyon floor (Fig. 2) accompanied by large (up to 5.5 Å) conformational changes in the HRV14 structure from the native conformation in the vicinity of the binding site. Here we report and contrast the structures of the virus–drug complexes for eight analogues (Fig. 1). We also report the structure of a drug-resistant mutant. An attempt is made to rationalize biological activity measured in terms of MIC and the properties of the drug-resistant mutants.

Data Collection, Reduction, and Calculation of Electron Density Maps

Cubic HRV14 crystals of diameter 0.25–0.45 mm (9) were soaked in solutions of the WIN compounds dissolved in dimethyl sulfoxide. The x-ray diffraction data were collected primarily at the Cornell High Energy Synchrotron Source (CHESS) and also (compound III) at the Brookhaven Laboratory's National Light Source. The resulting films were processed and scaled as described (10, 11). Processing statistics appear in Table 1.

Phase angles for the measured structure factor amplitudes of each virus–drug complex were obtained by the molecular-replacement real-space-averaging procedure (1, 12). Maps calculated by using these phases did not give clear images because the WIN compounds are not found at all available binding sites in the crystal. Rather, such a map represents the composite $k\rho_D + (1 - k)\rho_N$, where k is the occupancy of the WIN compounds, ρ_D is the electron density of the WIN compound–HRV14 complex, and ρ_N is the native HRV14 electron density in which the WIN compound is absent. To eliminate the contribution of ρ_N from the observed electron density map, the fraction $(1 - k)\rho_N$ was subtracted by using the native HRV14 amplitudes and native molecular replacement phases. The resulting "vector difference map," ρ_D, averaged over the 20 noncrystallographic copies, gave a clear image of the bound drug and the conformational changes in the drug-binding pocket. The value of k (Table 1) was refined by minimizing the R-factor (defined in Table 1) with respect to a model structure. These models have been refined by a version of the Hendrickson–Konnert procedure modified to incorporate the phase information derived from molecular replacement (13). Atomic coordinates derived from the interpretation of these electron density maps are being deposited with the Brookhaven Protein Data Bank simultaneously with publication of this paper (acquisition nos. 1RS1, 1RR1, 1RM2, 1RS3, 1R04, 1RS5, 1R06, 1R07).

Structures of the WIN Compound–HRV14 Complexes

All of the WIN antiviral agents are located at the same general site in the hydrophobic pocket beneath the canyon floor. This

The publication costs of this article were defrayed in part by page charge payment. This article must therefore be hereby marked "*advertisement*" in accordance with 18 U.S.C. §1734 solely to indicate this fact.

Abbreviations: HRV14, HRV2, HRV39, and HRV49, human rhinoviruses 14, 2, 39, and 49; VP, viral protein; MIC, minimal inhibitory concentration.

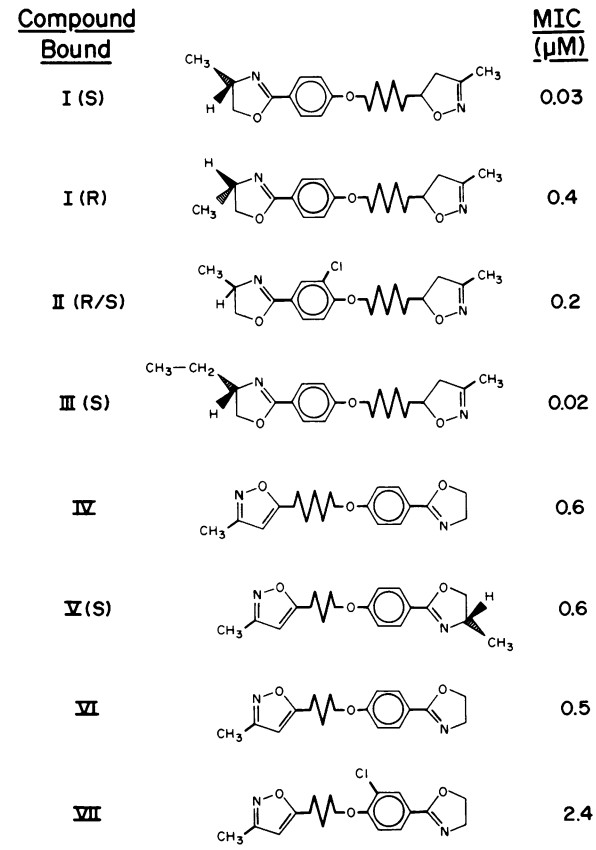

FIG. 1. Formula of antiviral compounds used in the studies reported here. Shown also are their *in vitro* activity against HRV14 measured in terms of the concentration (μM) required to reduce the plaque counts by a factor of 2 [minimal inhibitory concentration (MIC)].

pocket can be entered by way of a pore on the floor of the canyon (Fig. 2). The compounds with a seven-membered aliphatic chain and an aliphatic group (methyl or ethyl) on the oxazoline group that have been examined thus far bind in one orientation, while the other compounds examined here bind in the opposite direction (Fig. 1). Indicators of orientation are the relative size of the denser aromatic groups at either end and a constriction in the bigger density showing separation of the oxazoline–phenyl group and the site of the denser chlorine atoms in compound II and compound VII (Fig. 3). Previously it had been assumed that compound I(*S*) and compound IV were oriented in an identical way (8). The improved analytical procedures (described above) show that the predominant orientation of compound IV is in the opposite direction to that of compound I(*S*), with the positions of the isoxazole group and oxazoline–phenyl group exchanged. However, the clarity of the density for compound IV is not as good as that of any of the other compounds nor as that of the viral protein. Hence, it would seem possible that compound IV can bind in both directions, with a preference in the opposite sense to that of compound I(*S*). In the earlier analysis, it had been concluded that compound I(*S*) and compound IV had the same orientation because of the visibility of the additional methyl on compound I(*S*) in a difference map between these two compounds. Although this methyl gave rise to by far the largest positive feature in the difference map, there were other smaller positive as well as negative features in the vicinity of the WIN-binding pocket. The additional methyl of compound I(*S*) does not superimpose on any atom of the differently oriented compound IV, giving rise to the major feature in the difference map.

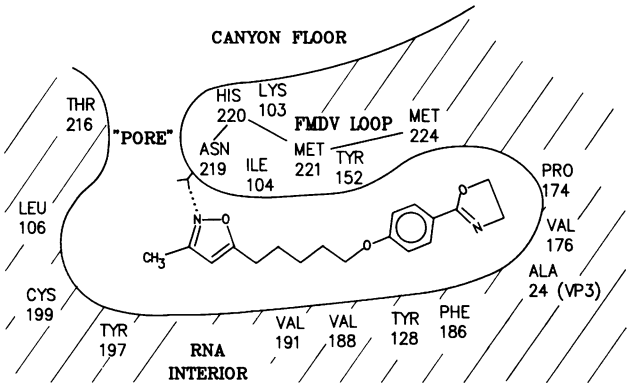

FIG. 2. Diagrammatic representation of compound VI bound in the WIN pocket. Note the orientation is opposite to that of compound I (8). Residues lining the pocket were selected as having atoms within 3.6 Å of any atom in compound I(*S*). This interior excludes H1245 shown in Fig. 3.

The interactions between the WIN compounds and the virus are almost entirely hydrophobic (Fig. 4). These compounds displace two water molecules from the WIN pocket, and the conformational changes induced primarily on the "FMDV loop" alter the binding sites of a further four water molecules. The electron density of all of the compounds is significantly lower in the aliphatic chain, suggesting that it might have a small degree of disorder. The occupancy of the compounds is roughly 60% in the crystal (Table 1), probably depending on the length of time of the crystal soak, the type of compound, and its solubility. There is no apparent preference of substitution at any of the 20 crystallographically independent sites in the virus.

The environments of compound II and compound VII (Fig. 4) represent the two major alternative and opposite binding modes, depending on the particular compound. The phenyl ring of compound VII (Fig. 4*B*) is roughly stacked between Tyr-1152[§] and Tyr-1128 and makes additional hydrophobic contacts with Val-1188 (shown but not labeled). Side chains from Phe-1186, Pro-1174, Met-1224, and Ala-3024 occupy the region around the oxazoline end of the drug. The isoxazole ring is stacked between the side chains of Tyr-1197 and Leu-1106 and forms a probable hydrogen bond with Asn-1219. A similar hydrogen bond between the oxazoline ring of compound II (Fig. 4*A*) and Asn-1219 has also been found. The shift in the position of the isoxazole ring in compound IV compared to compound VII (Fig. 4*B*) leads to two possible hydrogen bonds with the side chain of Asn-1219.

Of special interest is compound V with its additional methyl group on the oxazoline ring. Thus, it is like compound I but has an $n = 5$ instead of an $n = 7$ aliphatic chain. This compound binds at the closed end of the pocket and resembles the binding mode of compound VI. However, the additional methyl influences the location of the compound in the pocket, translating the whole structure by about 0.8 Å towards the "pore." The appearance of the electron density map and likely steric hindrances seen in the model is consistent with the *S* isomer used for soaking the crystals. In contrast, racemic mixtures were used for soaking the crystal with compounds I, II, and III. Compounds I and III showed preference for binding only the *S* enantiomer, consistent with MIC values about 1/10th that for their *R* enantiomer. The less active compound I(*R*) also has been studied independently and found to bind in a manner similar to compound I(*S*), except for the methyl group on the asymmetric carbon.

[§]In this manuscript, residues are labeled with a four digit notation. The first digit represents the viral protein (1, 2, 3, and 4), while the last three digits are the sequential amino acid number in that viral protein.

Table 1. X-ray diffraction data processing

Data	Compound bound									
	I(*S*)	I(*R*)	II(*R/S*)	III(*S*)	IV	V(*S*)	VI	VII	Val-188→Leu mutant	Native
Films used, no.										
0.3°	47	14	11	12	21	26	31	4	10	83
0.6°	12	0	0	0	8	0	0	0	0	0
Reflections measured	591,945	194,562	108,981	132,972	275,570	246,095	188,136	50,458	96,067	2,706,020
Basis for acceptance ($F^2 > ?\sigma$)	1σ	2σ	2σ	2σ	2σ	3.5σ	7σ	2σ	3σ	1σ
Unique reflections, no.	335,902	157,832	95,205	111,566	194,573	180,005	133,050	47,468	85,028	509,915
R factor*	11.0	11.5	13.7	17.0	13.6	11.1	10.7	14.4	11.6	11.0
Occupancy	0.45	0.65	0.60	0.55	0.50	0.70	0.65	0.55	–	–
Soaking time, days	1–1.5	7	7	0.5	1–1.5	7	2	7	–	–
Enantiomers used for soaking	*R/S*	*R*	*R/S*	*R/S*		*S*				

*$R = \dfrac{\sum_h \sum_i |(F_h^2 - F_{hi}^2)|}{\sum_h \sum_i F_h^2} \times 100$, where F_h^2 is the mean of i observations F_{hi}^2 for reflection h.

Compound II resembles compound I but with an additional chlorine on the phenyl group. The binding position would appear to be almost identical to that of compound I, with the chlorine pointing into the "top" of the binding pocket. This chlorine atom approaches the main chain and part of the side chain of residue Ile-1104 on one side and has the side chain of Met-1221 on the other. Compound VII is analogous to compound VI but with an additional chlorine on the phenyl group. It binds in the same orientation as compound VI except for a slight displacement of the aliphatic chain. In this case, the chlorine points towards the "top" of the binding pocket, interacting with the side chain of Tyr-1128 on one side and parts of the side chains of Ile-1104, Trp-1102, and Met-1224.

When the WIN compounds are bound, three stretches of the VP1 polypeptide chain occupy conformations distinctly different from the native HRV14 structure. The residues between 1213 and 1224 (Fig. 5*A*) (part of the chain leading from the "FMDV loop" to βH) are pushed out of the drug-binding site by distances of up to 4.5 Å in C^{α} positions (Fig. 6). A smaller but still considerable displacement (Fig. 5*B*) of residues 1151–1159 is also evident. Even smaller changes are found for the region between residues 1100 and 1110. The conformational changes were found to be largely independent (less than 0.2 Å for any main-chain atom) of the particular compound bound to the virus. The three displaced chain segments are associated with the β-sheet forming one side of the VP1 β-barrel. Hence, the conformational changes induced by drug binding are a concerted effect, causing the systematic movement of a β-sheet (Fig. 6). There appear to

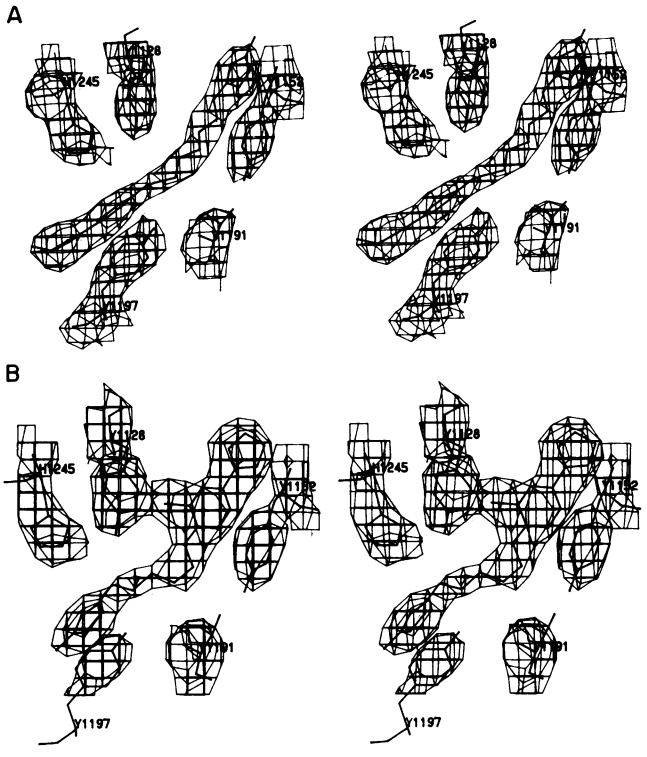

FIG. 3. Electron density showing compound I(*S*) (*A*) and compound VII (*B*). Note that the chlorine atom of compound VII readily defines the compound's orientation, although the larger volume of density for the phenyl–oxazoline group compared to the isoxazole group is also abundantly clear in both cases. The two compounds differ in the length of their aliphatic chains.

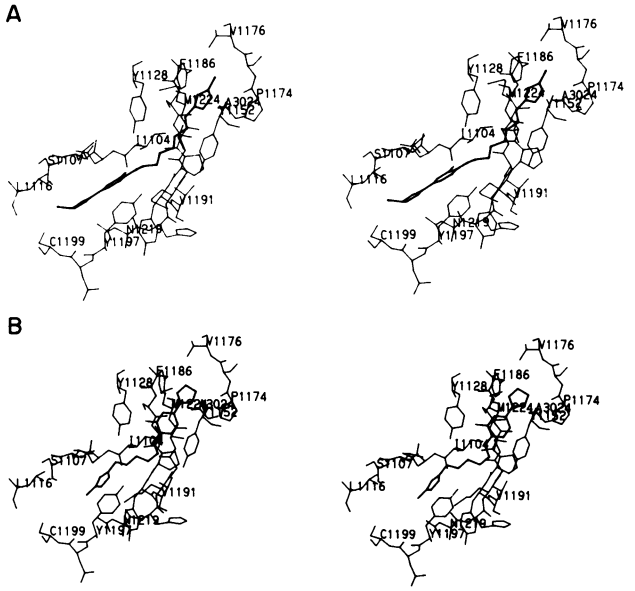

FIG. 4. Protein environment of bound compound II (*A*) and compound VII (*B*). Both of these compounds contain chlorine atoms, but they differ in the lengths of their aliphatic chain, the presence of a methyl substituent on the oxazoline group of compound II, and in their orientation within the binding pocket.

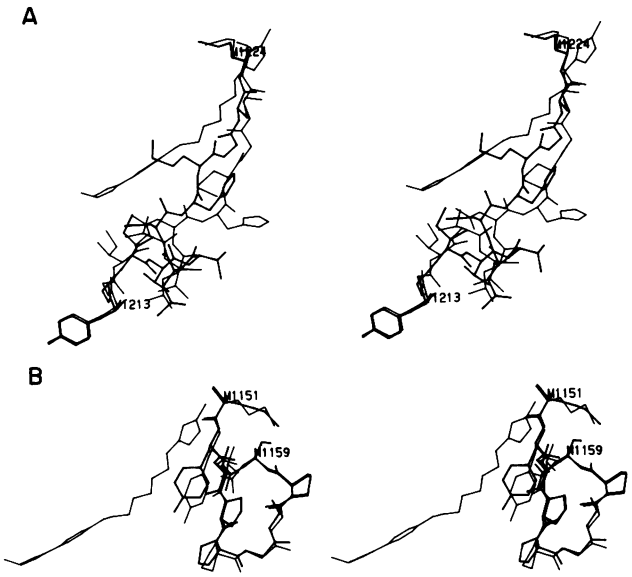

FIG. 5. Superposition of native HRV14 (heavy line) and the viral conformation altered by drug binding (light line): residues 1213–1224 (*A*) and residues 1151–1159 (*B*).

be two distinct energy minima corresponding to the native and drug-bound conformations.

Drug-Resistant Mutants

Two classes of drug-resistant mutants have been identified: a high-resistance class that replicated efficiently in high concentrations of drug (18 μg/ml), and a low-resistance class that could replicate only in low (0.3 μg/ml) concentrations of drug. The frequencies of the high-resistance mutants (1 per 10^4 plaque-forming units) were consistent with expectations for single-step mutations. The latter rate corresponds to the frequency of mutations seen in the search for escape mutants to neutralizing antibodies (14). Indeed, they may be considered as escape mutants to the drug. Thus, it was anticipated that these mutants would have single amino acid substitutions.

High-resistance mutants were selected in the presence of compound IV and compound I. The sites of mutations were determined by sequencing the RNA in the region encoding amino acids that line the WIN-binding site. All mutants so far characterized have base substitutions in codons specifying amino acids 1188 (valine → leucine or methionine) or 1199 (cysteine → tryptophan, arginine, or tyrosine). Clone SW12, selected with compound IV (Table 2), has substituted leucine for Val-1188. This mutant propagated well and crystallized easily. A difference electron density map (Fig. 7) confirmed the identity of the mutated amino acid and also showed that

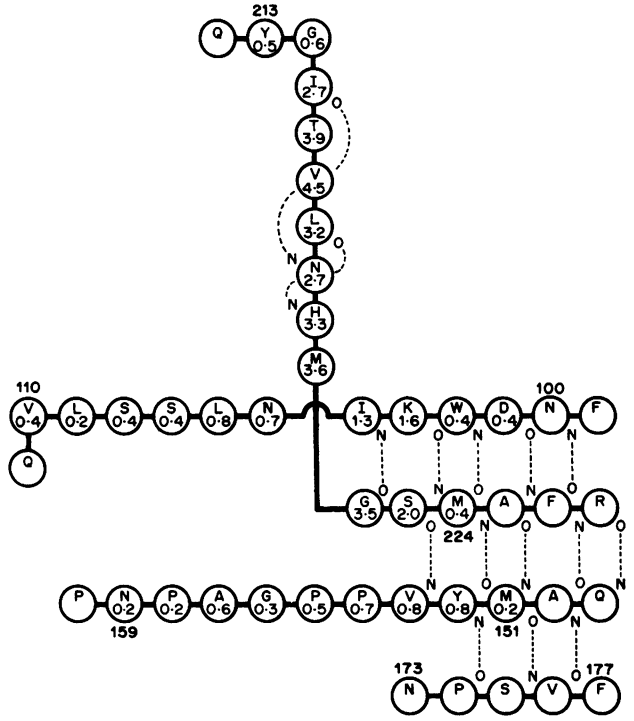

FIG. 6. Hydrogen bonding diagram of part of VP1 showing C^{α} displacement in Å of residues affected by drug binding. These residues are associated in a β-sheet and undergo a concerted movement independent of the particular bound drug.

there were no other visible mutations or conformational differences.

Fig. 8*A* shows the steric crowding of the phenyl group of compound IV (modeled as bound to wild-type virus) with the mutant leucine residue at position 1188 where the nearest approach is 1.9 Å. High MIC values (low activity) with compound IV were observed for mutant SW12, HRV2, HRV39, and HRV49, all of which have a leucine at the homologous position to 1188 in HRV14 (Table 2). However, compound I(*S*) is more active with respect to the mutated HRV14 virus. Therefore, it is of interest that the aliphatic chain of compound I would have relatively little steric hindrance (nearest approach is 2.9 Å) with a leucine at position 1188 (Fig. 8*B*) because of the opposite orientation of compound I to compound IV. Similarly, compound I has a much greater activity than compound IV in HRV2, HRV39, and HRV49, demonstrating that the opposite orientation of compounds IV and I observed crystallographically is roughly consistent with their observed antiviral activity. These observations break down for the shorter $n = 5$ chain compounds, which have relatively high activity in HRV2. This might be the result of other compensating changes in HRV2 and the possibility that these compounds do not fully penetrate to the

Table 2. Effect of mutations on MIC values

			MIC of compounds, μM					
	Residue		$n^* = 7$			$n^* = 5$		
Virus	1199	1188	I(*S*)	I(*R*)	IV	VI	V	VII
HRV14 wild type	Cys	Val	0.03	0.4	0.6	0.5	0.6	2.4
HRV14 mutant WIS 2-9†	Trp	Val	3.6	6.5	9.1	2.5	1.5	2.9
HRV14 mutant SW12	Cys	Leu	1.6	>10	>20	3.1	>10	>20
HRV2	Met	Leu	0.1	>10	4.1	1.5	0.1	0.1
HRV39	Met	Leu	1.0	>10	>20	2.9	0.6	0.4
HRV49	Met	Leu	0.3	3.1	4.4	2.0	0.3	0.2

*n = 7- and 5-membered aliphatic chains.
†Results are consistent with 19 other independently isolated cysteine → tryptophan mutations.

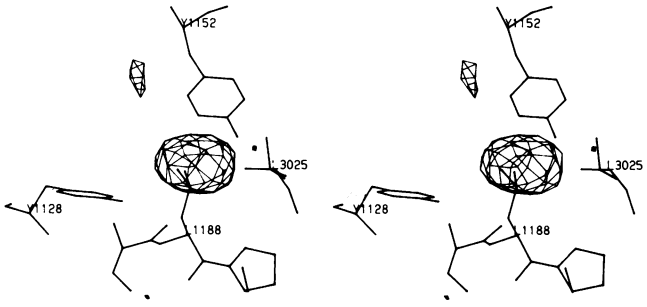

FIG. 7. Electron density difference map between mutant SW12 (Val-1188 → Leu) and wild-type virus. The positive peak at site 1188 had a height of 470 relative electron density units. The highest noise peak had a height of 186 units, and the negative peak where the valine used to be had a value of −216 units.

end of the WIN pocket. Similarly the greater loss of activity of compound I(*S*) compared to IV on mutating residue 1188 from valine to leucine cannot be explained readily.

The most commonly isolated mutation was cysteine to tryptophan at position 1199. The large tryptophan residue presumably sterically hinders the binding of compound I and compound IV (with respect to which the mutants were selected). Both of these compounds possess an $n = 7$-member-long aliphatic chain. However, compounds V and VI, with their shorter aliphatic chains of $n = 5$, bind at the closed end of the pocket in the wild type and presumably would not be expected to be hindered by the occurrence of the tryptophan residue (Fig. 8*C*). This is consistent with the observed retention of antiviral activity by these compounds against this mutant.

Conclusions

A rough understanding can be obtained of the relationship between biological MIC quantities and the binding mode, but it is unclear why compound I binds in the opposite direction to compound IV. The differences of antiviral activity appear to be a product of binding affinity, the mode of binding, and the delivery of the compound to the virus. In a previous paper (8), two possible mechanisms for the activity of the WIN compounds were suggested: (*i*) binding of the compounds might inhibit the flow of ions through the WIN pocket into the virus interior, which would cause swelling and disassembly; and (*ii*) binding of the compounds would stiffen VP1 and, therefore, inhibit the necessary flexibility for uncoating. Although the diffusion of heavy metal ions into the virus interior does occur (1), systematic analysis of the refined HRV14 structure does not reveal any special channels. Furthermore, the interior of the pocket, where the $n = 5$ compounds bind, would not be an optimal site for stopping ion flow. Thus, the ion-flow hypothesis now seems less probable. On the other hand, hypothesis *ii* has some confirmation in the light of the observation that the SW12 mutant (Val-1188 → Leu) is significantly more resistant to thermal inactivation in the presence of drugs than is wild-type virus (F.J.D., unpublished results). Thus, filling the pocket with WIN compounds or WIN compounds and larger amino acid side chains can improve stability and decrease uncoating potential.

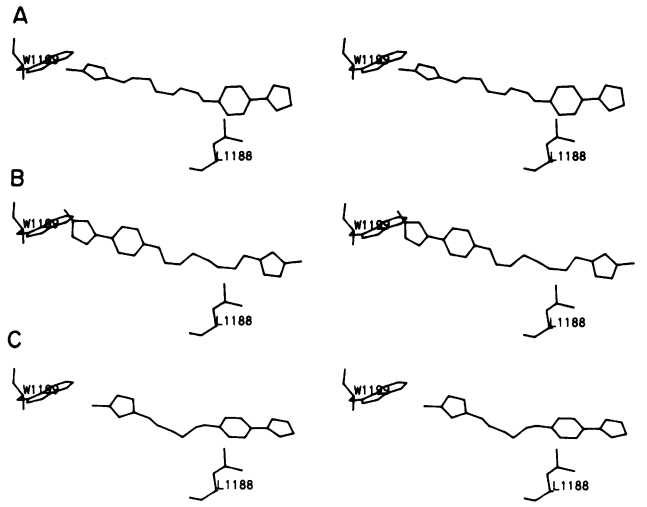

FIG. 8. Interaction of mutations at 1188 and 1199, selected for their resistance to the antiviral agents with compound IV (*A*), compound I(*S*) (*B*), and compound VI (*C*).

We are grateful to Sharon Fateley and Sharon Wilder for help in the preparation of the manuscript. We are most grateful for assistance by the staff of Cornell High Energy Synchrotron Source and Brookhaven National Laboratory Light Source in collecting our diffraction data. The work was supported by grants from the National Institutes of Health and the National Science Foundation as well as from the Sterling–Winthrop Research Institute.

1. Rossmann, M. G., Arnold, E., Erickson, J. W., Frankenberger, E. A., Griffith, J. P., Hecht, H. J., Johnson, J. E., Kamer, G., Luo, M., Mosser, A. G., Rueckert, R. R., Sherry, B. & Vriend, G. (1985) *Nature (London)* **317**, 145–153.
2. Hogle, J. M., Chow, M. & Filman, D. J. (1985) *Science* **229**, 1358–1365.
3. Luo, M., Vriend, G., Kamer, G., Minor, I., Arnold, E., Rossmann, M. G., Boege, U., Scraba, D. G., Duke, G. M. & Palmenberg, A. C. (1987) *Science* **235**, 182–191.
4. Diana, G. D., McKinlay, M. A., Otto, M. J., Akullian, V. & Oglesby, C. (1985) *J. Med. Chem.* **28**, 1906–1910.
5. Fox, M. P., Otto, M. J. & McKinlay, M. A. (1986) *Antimicrob. Agents Chemother.* **30**, 110–116.
6. Ninomiya, Y., Ohsawa, C., Aoyama, M., Umeda, I., Suhara, Y. & Ishitsuka, H. (1984) *Virology* **134**, 269–276.
7. Lonberg-Holm, K., Gosser, L. B. & Kauer, J. C. (1975) *J. Gen. Virol.* **27**, 329–342.
8. Smith, T. J., Kremer, M. J., Luo, M., Vriend, G., Arnold, E., Kamer, G., Rossmann, M. G., McKinlay, M. A., Diana, G. D. & Otto, M. J. (1986) *Science* **233**, 1286–1293.
9. Arnold, E., Erickson, J. W., Fout, G. S., Frankenberger, E. A., Hecht, H. J., Luo, M., Rossmann, M. G. & Rueckert, R. R. (1984) *J. Mol. Biol.* **177**, 417–430.
10. Rossmann, M. G. (1979) *J. Appl. Crystallogr.* **12**, 225–238.
11. Rossmann, M. G., Leslie, A. G. W., Abdel-Meguid, S. S. & Tsukihara, T. (1979) *J. Appl. Crystallogr.* **12**, 570–581.
12. Arnold, E., Vriend, G., Luo, M., Griffith, J. P., Kamer, G., Erickson, J. W., Johnson, J. E. & Rossmann, M. G. (1987) *Acta Crystallogr. Sect. A* **43**, 346–361.
13. Arnold, E. & Rossmann, M. G. (1988) *Acta Crystallogr.*, in press.
14. Sherry, B. & Rueckert, R. (1985) *J. Virol.* **53**, 137–143.